Korean J. Chem. Eng., 36(10), 1657-1668 (2019)
DOI: 10.1007/s11814-019-0359-y

pISSN: 0256-1115
eISSN: 1975-7220

A new type of [PEI-glycidyl POSS] nanofiltration membrane with enhanced separation and antifouling performance

Samaneh Bandehali, Abdolreza Moghadassi†, Fahime Parvizian, and SayedMohsen Hosseini

Department of Chemical Engineering, Faculty of Engineering, Arak University, Arak 38156-8-8349, Iran
(*Received 11 May 2019 • accepted 8 August 2019*)

Abstract−A new type of polyether-imide (PEI)-based nanofiltration membranes was prepared by introducing octa-glycidyloxypropyl-silsesquioxane (Glycidyl POSS) into PEI matrix for heavy metals ions removal from water. The separation performance of fabricated membranes in Na_2SO_4, $Pb(NO_3)_2$, $Ni(NO_3)_2$ and $Cu(NO_3)_2$ removal from water as well as their flux and antifouling property was evaluated. Fourier transform infrared spectroscopy (FTIR), field emission scanning electron microscopy (FESEM), energy dispersive X-ray (EDX) analytical method, atomic force microscope (AFM), porosity, contact angle, and water content were also used in membrane characterization. The results indicated higher hydrophilicity, pure water flux (PWF) and salt rejection for PEI-POSS membranes compared to neat PEI ones. The morphological images showed good tuning porosity, finger- and spongy-like structure. The highest porosity observed for [PEI-1 wt% glycidyl POSS] with the best antifouling property. The surface roughness also decreased by incorporating of POSS into PEI matrix. The pure water flux increased from 14.3 (L/m^2h) for neat PEI membrane to 36 (L/m^2h) for [PEI-0.1 wt% glycidyl POSS]. Moreover, Na_2SO_4, $Pb(NO_3)_2$, $Cu(NO_3)_2$ and $Ni(NO_3)_2$ rejection measured 78%, 94%, 99%, 42% for [PEI-1 wt% glycidyl POSS] membrane, whereas they were 69%, 44%, 40% and 16% for the virgin PEI membrane, respectively. Results showed a good potential for [PEI-POSS] membrane in Cu and Pb ions removal beside its high PWF and antifouling ability.

Keywords: Polyhedral Oligosilsesquioxane (POSS), Nanofiltration, Improved Flux, Heavy Metal Separation, Antifouling Property

INTRODUCTION

Membrane filtration processes such as ultrafiltration (UF), microfiltration (MF), nanofiltration (NF) and reverse osmosis (RO) have been developed and applied in wastewater treatment due to high efficiency in salt separation, low energy consumption, and ease of operation [1-3]. Among these, NF membranes are promising methods that have been developed in the last two decades. The separation process of different solutions by NF membranes is based on various mechanisms such as size sieving, steric hindrance, Donnan exclusion (electrostatic repulsion) mechanisms and dielectric effects that lead to selective separation of different ions. There are various approaches to improving separation performance of NF membranes by tuning membrane nano-pores between the size of organic molecules and salt ions through incorporation of organic and inorganic materials [4-7]. Polyhedral oligosilsesquioxane (POSS) is defined as a silica nanoparticle that contains silica cage core and functional groups. POSS as a unique 3D nanoparticle has been investigated in the past 50 years. The chemical structure of POSS is $(RSiO_{1.5})_n$ that R is vertex groups, such as halogen, alkene, aryl, alkyl, hydrogen, arylene [8]. Introducing POSS especially with epoxy groups into the polymer structure enhances thermal stability, permeability, glass temperature and non-flammability due to its rigid cage structure [9]. POSS shows good dispersity and compatibility with polymers as membrane matrix. Physical blending and chemical cross-linking are two approaches for incorporation of POSS into the polymer. POSS shows successful physical blending due to good dispersity and suitable polymer affinity. Ligands have an important role in the interaction between polymer and nanoparticles and spatial distribution of nanoparticles. Nevertheless, it has been used less for modification of nanofiltration membranes and more in preparation of gas separation and pervaporation membranes [10-12]. Some studies have been carried out on salt removal from water by incorporation of POSS into membrane matrix. Koutahzadeh et al. [13] investigated the incorporation of POSS into the polysulfone (PSf) as a membrane matrix for preparation of nanocomposite UF membranes. The membranes showed higher hydrophilicity compared with pure membranes. The longer finger-like pores formed in the top layer of the membrane surface enhanced water flux. The highest permeability was observed for POSS-PSf with 2 wt% POSS. The best results, such as good permeability and suitable antifouling properties and high humic acid (HA) rejection, were obtained for 0.5 wt% POSS compared with pristine PSf membranes. Dalwani et al. [14] applied POSS ammonium salt as an aqueous monomer and 1, 3, 5-benzenetricarbonyltrichloride (TMC) as an organic monomer for preparation of a thin POSS-polyamide membrane with high separation performance. Duan et al. [15] used four kinds of POSS with various functional groups (P-8NH_2, P-1NH_2, P-8NH_3Cl, and P-8Phenyl) in the selective layer for seawater desalination.

Chen et al. [16] investigated polybenzimidazole (PBI)-(POSS)/

†To whom correspondence should be addressed.
E-mail: a-moghadassi@araku.ac.ir

polyacrylonitrile (PAN) hollow fiber membranes for forward osmosis (FO) and pressure retarded osmosis (PRO) process applications. The FO and PRO were investigated for $CaSO_4{\cdot}2H_2O$ gypsum scaling as inorganic fouling and sodium alginate fouling as organic fouling. The results showed that gypsum scaling can be eliminated by improving reverse $MgCl_2$ flux because of competition between $MgSO_4$ and $CaSO_4{\cdot}2H_2O$. Moreover, by increasing the reverse NaCl flux, alginate fouling did not produce significant alterations in both processes. The flux of permeate illustrated a major role in the control of fouling. Thus, lower fouling occurred for the PRO process. Sun et al. [17] reported the synthesis of EG-POSS as an additive by the grafting between ethylene glycol (EG) for preparation of polyvinylidene fluoride (PVDF)/EG-POSS. Incorporation of EG-POSS enhanced hydrophilicity and antifouling properties on the membrane surface and the highest pure water flux observed for 0.5% EG-POSS. Recently, You et al. [18] reported the functionalization of POSS by polyethylene glycol for fabrication of polyamide-based NF membranes. They applied interfacial polymerization trimesoyl chloride (TMC) and piperazine (PIP) on a UF substrate of polyethersulfone. The charge and hydrophilicity of membrane surface improved compared with pure polyamide membrane. The highest PWF obtained was 38.7 (Lm^{-2} h^{-1}) at 0.2 MPa without reducing Na_2SO_4 rejection with value (87.1-91.6%). In another work, You et al. [4] used amine functionalized-POSS nanoparticles for tuning nanopores in the polydopamine (PDA) membrane. The nanoporosity size decreased in the range of 1.04-1.07 nm. The best permeation was 1,099 $Lm^{-2}h^{-1}MPa^{-1}$ with dye and salt rejection above 90%. Liu et al. [19] reported the polyamide (PA)/POSS hybrid membranes with excellent anti-chlorine and anti-bacterial properties in RO applications. POSS was in situ armored on the PA membrane and acted as armor to improve membrane resistance against active chlorine corrosion and bacterial fouling. The rejection of NaCl reached 98% after membrane immersion into chlorine solution for 24 h.

Bahrami et al. [20] used octa-aminopropyl polyhedral oligomeric silsesquioxane hydrochloride salt (OA-POSS) nanoparticles-based calcium-alginate/polyacrylamide (Alg/PAAm) double network (DN) hydrogel. The mechanical property of gels was increased by incorporation of OA-POSS nanomaterials. Alg/PAAm/OA-POSS gels were applied to adsorption of dye from wastewater. Lu et al. [21] fabricated the omniphobic nanofiber membrane for the application of membrane distillation by electrospinning of polyvinylidenefluoride-co-hexafluoropropylene (PVDF-HFP) and fluorinated-decyl polyhedraloligomeric silsesquioxane (F-POSS) colloidal suspension solution. The high concentration of F-POSS was placed on the surface of F-POSS/PVDF-HFP membranes. These membranes showed good omniphobicity properties and high PWF at low surface tension. Yamamoto et al. [22] reported the preparation of POSS (polyhedral oligomeric silsesquioxane)-containing silica sols by hydrolysis/condensation of octakis(triethoxysilylethyl)-substituted POSS (TESE-POSS) and mixtures of 1, 2-bis (triethoxysilyl) ethane (BTESE1) and TESE-POSS in $HCl/H_2O/EtOH$. The surface area of gels was 168-424 m^2/g with porous structure. Then, they were coated on $SiO_2/ZrO_2/TiO_2$ porous supports and calcinated at 350 or 400 °C to produce the membranes. These membranes showed high performance in RO application. The results showed NaCl rejection ~90% for 2,000 ppm NaCl aqueous solution.

Heavy metal ions as toxic elements such as lead (Pb), nickel (Ni) and copper (Cu) are the major pollutants in the reservoirs of freshwater. Industrial wastes are the main source for heavy metal pollutants. Therefore, developing treatment technologies with high efficiency has gained much attention [23].

POSS has a high potential for adsorption of heavy metals such as selenium and arsenic, as shown by He et al. [24]. They reported preparation of POSS-polyamide membranes by interfacial polymerization between piperazine (PIP) and 1, 3, 5-benzenetricarbonyltrichloride (TMC). The membranes were applied to separation of arsenic and selenium. The fabricated membranes showed high rejections of SeO_3^{2-}: 93.9, SeO_4^{2-}: 96.5, and $HAsO_4^{2-}$: 97.4%. Asuman Celik and Oya Aydın [25] reported the high potential of PGE-POSS and chitosan nanocomposite materials for adsorption of cadmium (Cd (II)) from wastewater due to increasing active sites, good solubility and dispersibility of POSS molecules.

In this study, polyether-imide/glycidyl POSS nanofiltration membranes were developed by phase inversion method. Polyether-imide (PEI) was considered as membrane matrix due to its high thermal and mechanical stability, excellent chemical resistance, low cost, and excellent film-forming ability. PEI is a hydrophobic polymer that shows low rejection that limits its application in wastewater treatment due to decreased fouling resistance. Therefore, enhancement of fouling resistance and hydrophilicity property of membrane are important challenges in preparing NF membranes. Membrane hydrophilicity can be improved by some techniques such as grafting, tailoring, blending, introducing organic and inorganic materials [26-28]. In this study, the influences of glycidyl-POSS into the PEI as membrane matrix on physico-chemical properties and separation performance of them were investigated. The ability of [PEI-POSS] membrane in Na_2SO_4, Pb $(NO_3)_2$, Ni $(NO_3)_2$ and Cu $(NO_3)_2$ removal from water, antifouling property as well as its permeability and separation performance was studied. The physico-chemical properties of prepared membranes were characterized by FTIR, FESEM, EDX, AFM, porosity measurement, contact angle and water content.

MATERIALS AND METHODS

1. Materials

Polyetherimide (PEI) (M_w: 35,000 Da), was obtained from Sigma Aldrich. The N, N-dimethylacetamide (DMAc) was purchased from DAEJUNG, Korea. Octaglycidyloxypropyl-silsesquioxane (glycidyl POSS) purchased from Iran Polymer and Petrochemical Institute. The polyvinylpyrrolidone (PVP) was also purchased from Merck. Aqueous solutions of Na_2SO_4, $Pb(NO_3)_2$, $Ni(NO_3)_2$ and $Cu(NO_3)_2$ were applied as feed solutions for studies of membrane separation. The chemical structure of glycidyl POSS and polyetherimide are shown in Fig. 1.

2. Membrane Preparation

PEI/glycidyl POSS membranes were prepared by phase inversion method via immersion into the deionized water bath. For the purpose, glycidyl POSS with different concentrations (up to 1 wt%) was dispersed in DMAc solvent and stirred for 1 h at ambient temperature. PEI with the ratio of 18 wt% of total polymer concentra-

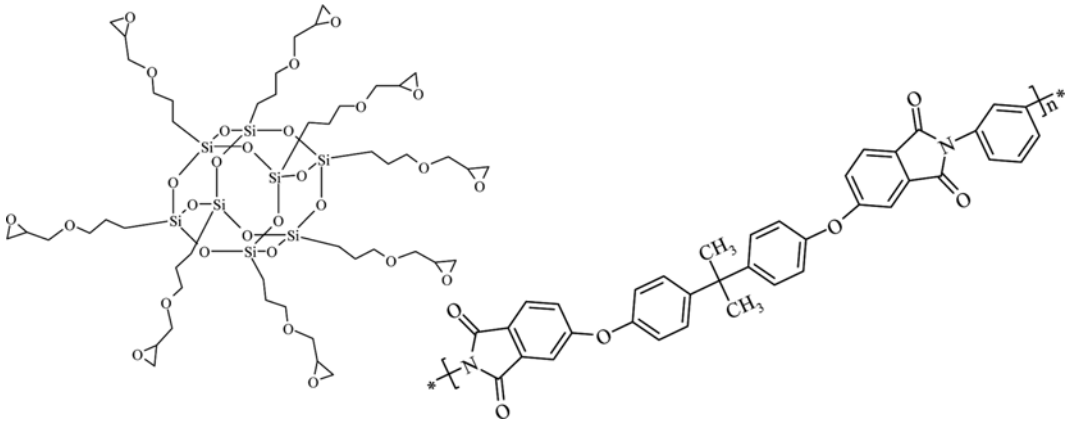

Fig. 1. The chemical structure of octaglycidyloxypropyl-silsesquioxane (glycidyl POSS) and polyether-imide.

Table 1. The casting solution composition used for preparation of membranes

Membrane	PEI (wt%)	DMAc (wt%)	G-POSS (wt%)	PVP (wt%)
M0	18	81	0	1
M1	18	80.999	0.001	1
M2	18	80.99	0.01	1
M3	18	80.9	0.1	1
M4	18	80	1	1

tion in the solution of final casting was added to the dispersed solution in the prior step. Moreover, 1 wt% of polyvinyl pyrrolidone (PVP) was used as a pore-forming agent. Then, the casting solution was stirred for 18 h at 65 °C to achieve a homogeneous solution. The prepared solution was kept 8 h without stirring at the same temperature to remove trapped air bubbles. The casting solution was spread on a clean glass plate and cast by an applicator with the thickness of 150 μm. Then it was soaked in a water bath (deionized water) for complete phase inversion. Table 1 shows the details of membrane compositions.

3. Membrane Characterization

Fourier transform infrared spectroscopy (FTIR) was used to confirm the presence of glycidyl POSS in the membranes. FTIR spectra were recorded with a Bruker spectrometer (TENSOR 27) in the range of 500 to 4,000 cm^{-1} at a resolution of 1 cm^{-1} for each spectrum. The morphology of membranes was characterized by FESEM. Before analysis, samples were dried and fractured in liquid nitrogen. By using the sputtering device, samples were smeared with gold in order to obtain conductance.

Also, the X-ray elemental mapping analysis of Si on the membrane surface was performed to understand the distribution of glycidyl POSS. Atomic force microscopy (AFM) was used for detection of membrane surface roughness. The scanning area for AFM images was set at 8 μm×8 μm. The overall porosity of membrane (ε) was measured by the equation:

$$\varepsilon(\%)=\left(\frac{W_w-W_d}{\rho_f V_m}\right)\times 100 \tag{1}$$

where W_d and W_w are the weight of dry and wet membranes (g). The ρ_f and V_m are also water density (g/cm^3) and membrane volume (cm^3), respectively. For decreasing experimental errors, all the experiments were done three times and the average values were considered. Furthermore, water contact angle study was used to investigate the membrane surface hydrophilicity.

The mean pore sizes were determined by Guerout-Elford-Ferry equation [29-31]:

$$r_m=\sqrt{\frac{(2.9-1.75\varepsilon)8\eta LQ}{\varepsilon A\Delta p}} \tag{2}$$

where η, Q and ΔP are the water viscosity (8.9×10^{-4} Pa·s), the volume of the permeated pure water flux (m^3/s), and operating pressure (0.45 MPa), respectively. L is the membrane thickness (m), A is the membrane filtration area (m^2), and ε is the surface porosity.

4. Membrane Separation Performance Analysis

The membrane separation performance was evaluated by a dead-end NF cell. At first, all membranes were compacted with water for 1 h to obtain steady-state conditions. The membranes were tested at 25 °C and 4.5 bar. The water flux was determined by:

$$J_{w,1}=\frac{V}{A\times T} \tag{3}$$

where $J_{w,1}$, V, A and T are the permeate flux ($Lm^{-2}h^{-1}$), the volume of solution or water permeates, the effective area of membrane (11.94 cm^2) and time (h), respectively.

Aqueous solutions of Na_2SO_4, $Pb(NO_3)_2$, $Ni(NO_3)_2$ and $Cu(NO_3)_2$ were used as feed to evaluate nanofiltration performance. The salt rejection was calculated by Eq. (4) as follows:

$$R(\%)=\left(1-\frac{C_p}{C_f}\right)\times 100 \tag{4}$$

where the concentration of feed solution and permeate are C_f and C_p, respectively.

After that, fouled membranes due to having a high concentration of salts were taken into the deionized water for 2 h and were washed. Then the permeation of pure water flux ($J_{w,2}$ (L/m^2h)) was measured again for evaluation of membrane fouling. The flux recovery ratio was calculated by Eq. (5):

$$FRR\% = \left(\frac{J_{w,2}}{J_{w,1}}\right) \times 100 \quad (5)$$

All the experiments were carried out three times and the average values were reported to reduce experimental errors.

RESULTS AND DISCUSSION

1. Characterizations of the Membranes

1-1. ATR-IR and FTIR Analyses

The presence of glycidyl-POSS was verified by attenuated total reflectance infrared (ATR-IR) spectroscopy. FT-IR analysis is shown in Fig. 2 in the range of 600-4,000 cm^{-1} with resolution 4 cm^{-1}. Two peaks in the range of 1,100 and 1,054 cm^{-1} are due to the cage structure of Si-O-Si groups, and in the range of 2,868 and 2,933 cm^{-1} attributed to glycidyl groups. Moreover, the AT-IR spectra PEI/glycidyl POSS hybrid membranes show the peak around 1,780 cm^{-1} that is attributed to C=O asymmetric stretch of imide groups), 1,720 cm^{-1} (attributed to C=O symmetric stretch of imide groups), 1,357 cm^{-1} attributed to C-N stretch of imide groups [26,32,33].

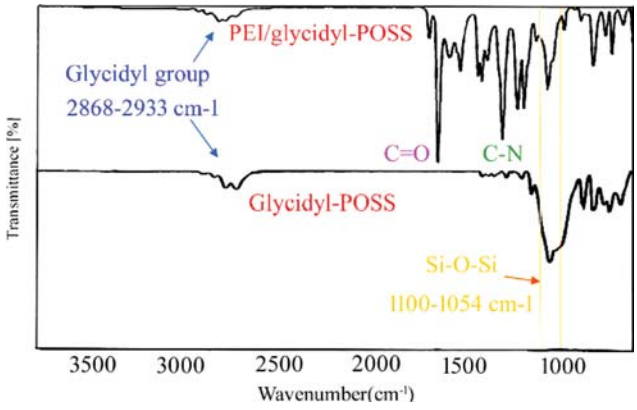

Fig. 2. ATR-IR and FTIR spectra of PEI/glycidyl-POSS membranes and glycidyl-POSS.

1-2. Membrane Morphology

Fig. 3 shows the FESEM images for the pristine and blended glycidyl-POSS/PEI membranes. The cross-section images show the asymmetric structure including a selective layer and a finger-like structure with micro-voids in the thicker layer of support. This structure of membranes is due to immersion of membrane into the bath and solvent replacement with non-solvent during the phase

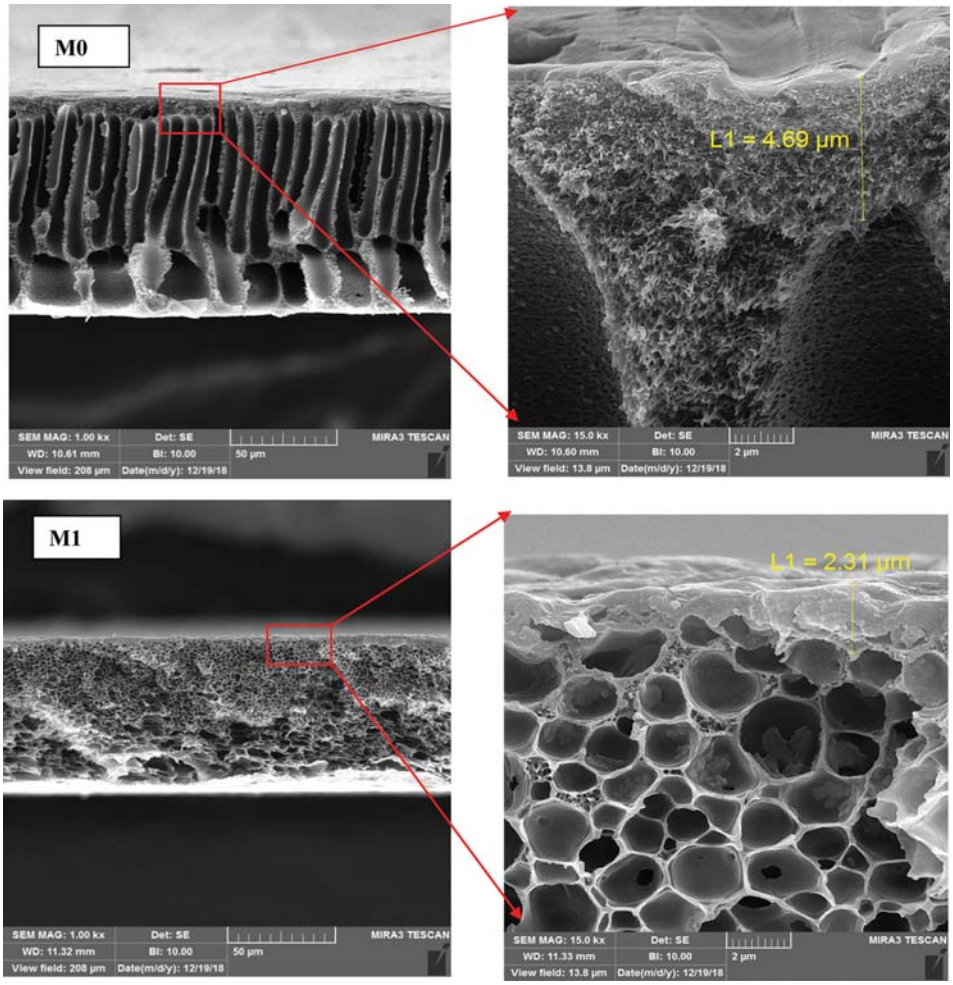

Fig. 3. FESEM cross-section images of prepared membranes.

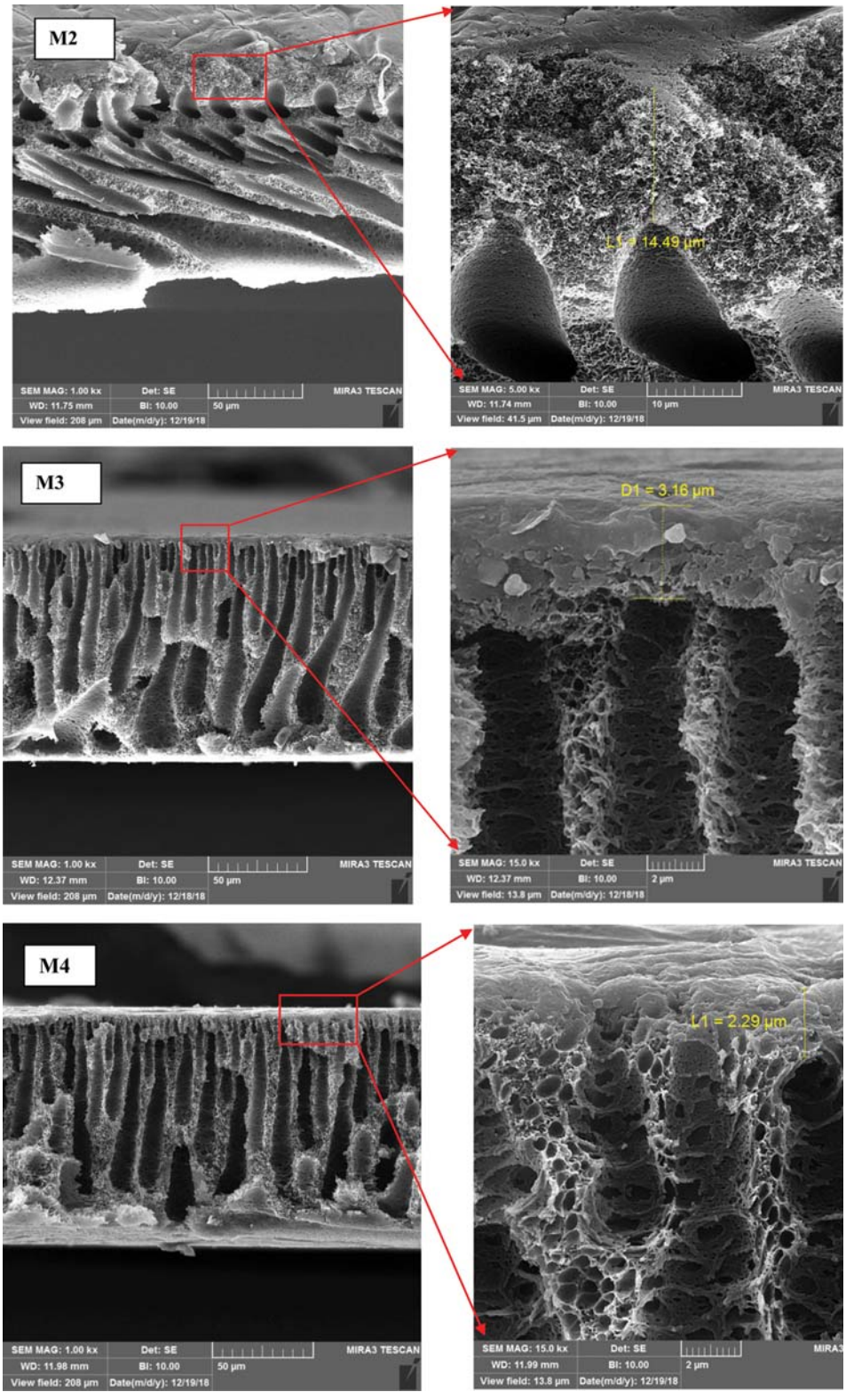

Fig. 3. Continued.

inversion process. The FESEM images showed that increasing the glycidyl-POSS into the membranes increased porosity and micro-voids with the suitable finger- and spongy-like structure. The structure of M2 is different from other fabricated membranes, and it shows spongy-like structure due to low solubility and high viscosity of glycidyl POSS. Therefore, glycidyl-POSS participated slowly, so that its result is the formation of spongy-like structure [27,34,35]. The influence of glycidyl-POSS in the top layer of membranes is

the enhancement of skin layer resistance by increasing the thickness of the top layer, and the size of the micro-voids increases with increasing glycidyl-POSS that leads to improving PWF. The thickness of the top layer increased from 4.69 μm in M0 to 14.49 μm in M2. Then it decreased to 2.22 μm in a high concentration of glycidyl POSS (M4) due to increase solution viscosity and delay exchange between non-solvent and solvent in the phase inversion process. Moreover, precise tuning of structure into membranes and pores is clear in the images with the application of glycidyl POSS. In high concentration of glycidyl POSS, the size of porosities decreases due to aggregate glycidyl POSS, that is clear for M4 [13,31,36]. The pore structures depend on the rate of phase inversion. By increasing the glycidyl-POSS the formation of pores is related to the equilibrium between kinetic (viscosity) and thermodynamic (miscibility) effects during the phase inversion process. Glycidyl-POSS with organic and inorganic structure into the phase inversion process can be delayed or accelerated due to the molecular weight of polymer and solubility of polymer-particle. The rapid de-mixing process occurs in lower viscosity, which leads to increased finger-like structure pores. By incorporation of glycidyl-POSS in 0.001 wt% increases the casting solution viscosity compared to pure PEI and then leads to delay phase inversion process and spongy-like structure. However, in a higher concentration of glycidyl-POSS, the viscosity of casting solution increases, but the more negative charges on the membrane surface increase the speed of phase inversion process due to forming hydrogen bonds, the result of which is more finger-like structure of the membrane. This structure is revealed for M2, M3, and M4. As shown in Fig. 3, the NF membranes content 1 wt% glycidyl-POSS have competition in the effects of kinetic (viscosity) and thermodynamic (miscibility). Therefore, the long finger structure forms due to more effects of thermodynamic and reducing miscibility of thermodynamic effects into the casting solution and increased liquid-liquid mixing [13]. Furthermore, mapping analysis was carried out for confirmation of Si element present and the distribution of glycidyl-POSS into the membrane structure that is shown in Fig. 4.

1-3. Surface Roughness and AFM Images of the Membranes

The images of AFM for prepared membranes are shown in Fig. 5 for pure and hybrid membranes in scanning area 8 μm×8 μm. The surface roughness parameters are illustrated in Table 2. The surface morphology of prepared membranes was changed by increasing the amount of glycidyl-POSS. The membrane roughness

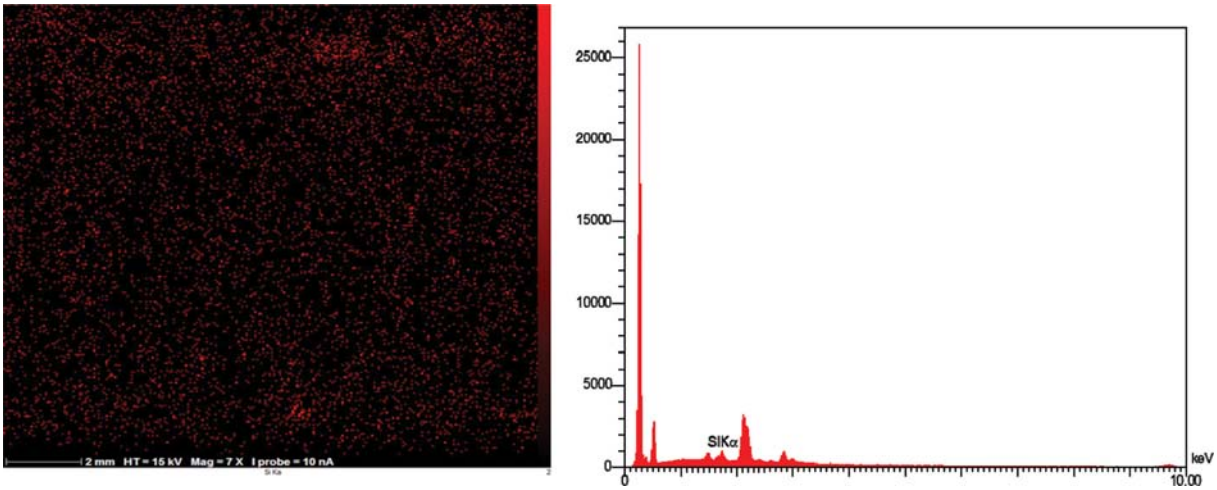

Fig. 4. Mapping analysis for 1 wt% glycidyl POSS of prepared membranes.

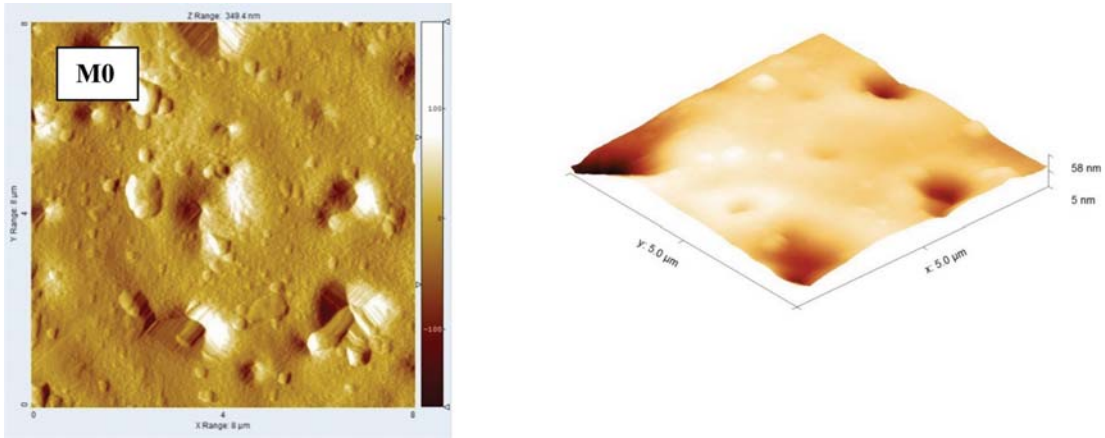

Fig. 5. Three- and two-dimensional AFM images for the fabricated membranes.

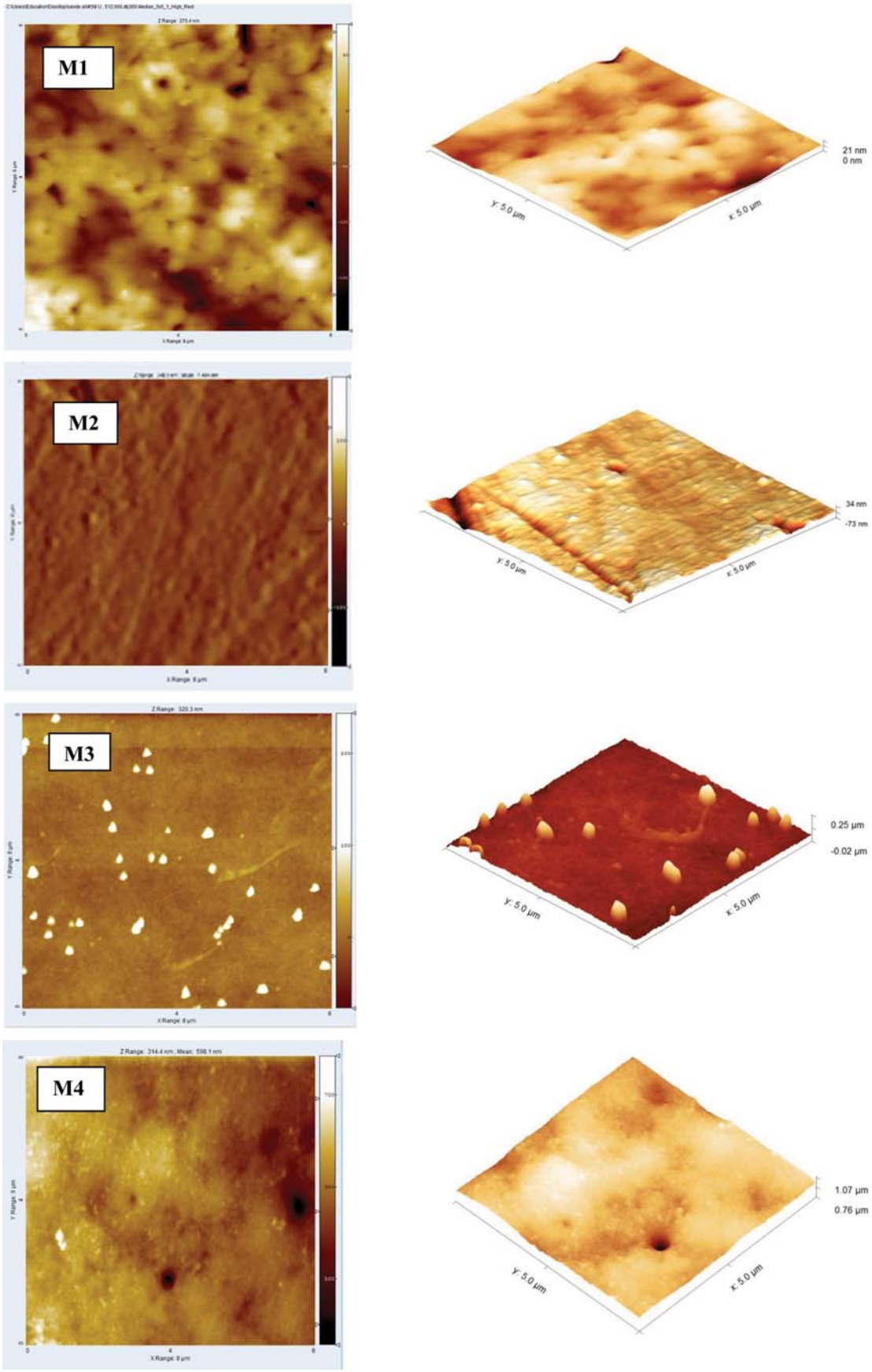

Fig. 5. Continued.

Table 2. The roughness parameters for the prepared membranes

Sample	R_a	R_q
M0	57.7 nm	82.8 nm
M1	27 nm	33 nm
M2	23 nm	30 nm
M3	19.17 nm	19.1 nm
M4	19.49 nm	23.44 nm

also decreased by increase of glycidyl-POSS. The roughness of membranes is expressed in terms of the average membrane roughness (R_a) and the root mean square of the height data (R_q). The average roughness of membranes decreased compared with pure PEI due to replacing glycidyl-POSS between pores of membrane surface that leads to a smoother surface. Then membrane roughness increased in high concentration (1 wt% glycidyl-POSS) due to aggregate glycidyl POSS on the membrane surface [13,37,38].

The membrane porosity and mean pore size of the membranes are shown in Table 3. The highest membrane porosity (81%) is indicated for M4 at 1 wt% glycidyl-POSS. Moreover, the mean pore size of the membrane decreased in M4, which can be explained in the result of filling pores with glycidyl-POSS.

1-4. Contact Angle

The water contact angle was measured to investigate membrane hydrophilicity. The angle between flat horizontal surface and water droplet shows that higher hydrophilic membranes have a lower contact angle. The contact angle for neat and hybrid membranes is shown in Fig. 6. It is clear from Fig. 6, by increasing glycidyl-POSS decreased contact angle from 65° for the neat membrane to 29° for PEI/ glycidyl POSS (0.1 wt%) and enhanced membrane hydrophilicity. Improvement of hydrophilicity can be the result of tuning membrane porosity and formation the nanostructure of glycidyl-POSS and simple transport of water molecules and hydrogen bonding between epoxy groups and water molecules. By increasing the concentration of glycidyl POSS (M4), the water contact angle was increased due to filling porosities with glycidyl POSS and poor distribution of glycidyl POSS and blockage water routes.

1-5. Water Content of Membranes

The water content measurements of membranes are a criterion of swelling and hydrophilicity [39-41]. Table 4 shows the values of water content for all prepared membranes. According to Table 4, the increase of glycidyl-POSS increased water content in M1 compared with neat PEI due to hydrophilic cage structure of glycidyl-POSS. But water content decreased from 0.001 wt% (M1) to 0.01 wt% (M2) due to decrease of porosity. Then by more increase of glycidyl-POSS, the water content reached 71% due to increase of membrane heterogeneity.

2. Prepared Membrane Performance

2-1. Pure Water Flux

Fig. 7 shows the changes of pure water flux (PWF) at different glycidyl-POSS concentrations. The highest PWF (36 L/m^{2}h) was

Table 3. Mean pore size, porosity and flux of the prepared membranes

Membrane	Mean pore size (m)	Porosity (%)
M0	1.07E-09	58
M1	1.56E-09	70
M2	1.94E-09	57
M3	2.35E-09	61
M4	1.20E-09	81

Table 4. The effect of glycidyl POSS on the membranes water content

Glycidyl-POSS concentration (wt%)	Water content (%)
0	67
0.001	72
0.01	63
0.1	66
1	71

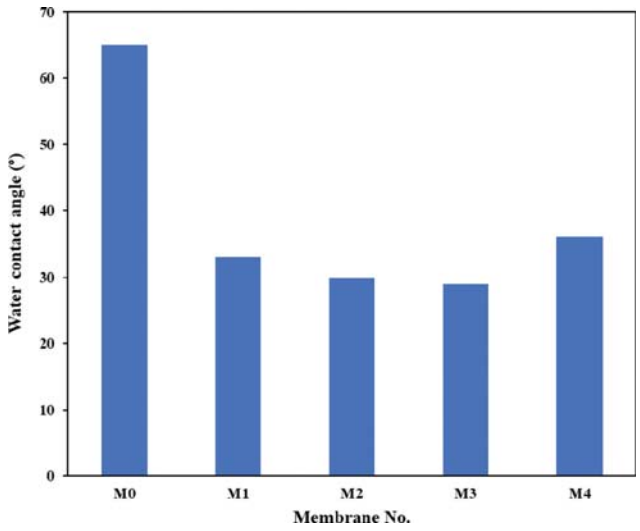

Fig. 6. Water contact angle of the prepared membranes.

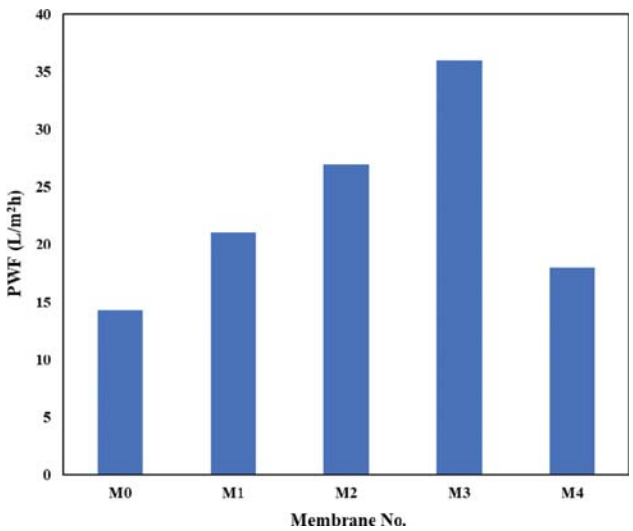

Fig. 7. Pure water flux for the prepared membranes.

observed for M3 which had ~60% increase compared with pristine PEI due to presence of hydrophilic epoxy groups and formation of hydrogen bonding with water molecules. Moreover, M3 shows the highest mean pore size of the membrane according to Table 3, which led to increase of PWF. Then PWF decreased to 18 L/m^{2}h at 1 wt-POSS. However, the porosity increased in M4 but the decreasing PWF is attributed to the high concentration of glycidyl-POSS into the membrane matrix and pores blockage and sharply decreasing mean pore sizes of M4 that led to reducing PWF. Moreover, the POSS materials are hydrophobic, and hydrophobicity overcomes the hydrophilicity of epoxy groups in a high concentration of glycidyl POSS [15]. Therefore, PWF was reduced by decreasing hydrophilicity in 1 wt% glycidyl POSS. The results are in good agreement with the contact angle data. Generally, by incorporation of glycidyl-POSS, the PWF improved from M0 to M3 due to size tuning of membrane porosity and increasing pores sizes among blended membranes and enhanced membrane wettability due to the attraction between water molecules and membrane.

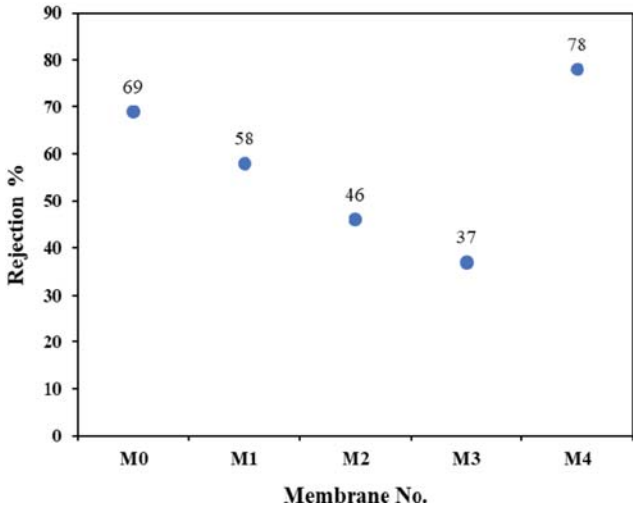

Fig. 8. The salt rejection of the prepared membranes for Na_2SO_4, aqueous solutions.

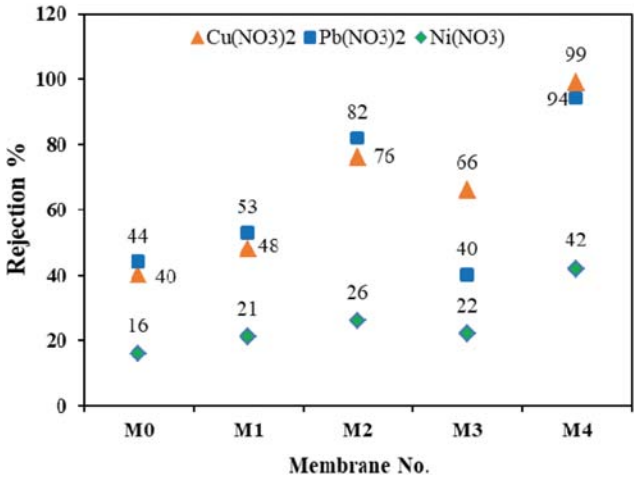

Fig. 9. The $Pb(NO_3)_2$, $Cu(NO_3)_2$ and $Ni(NO_3)_2$ rejection for the prepared membranes.

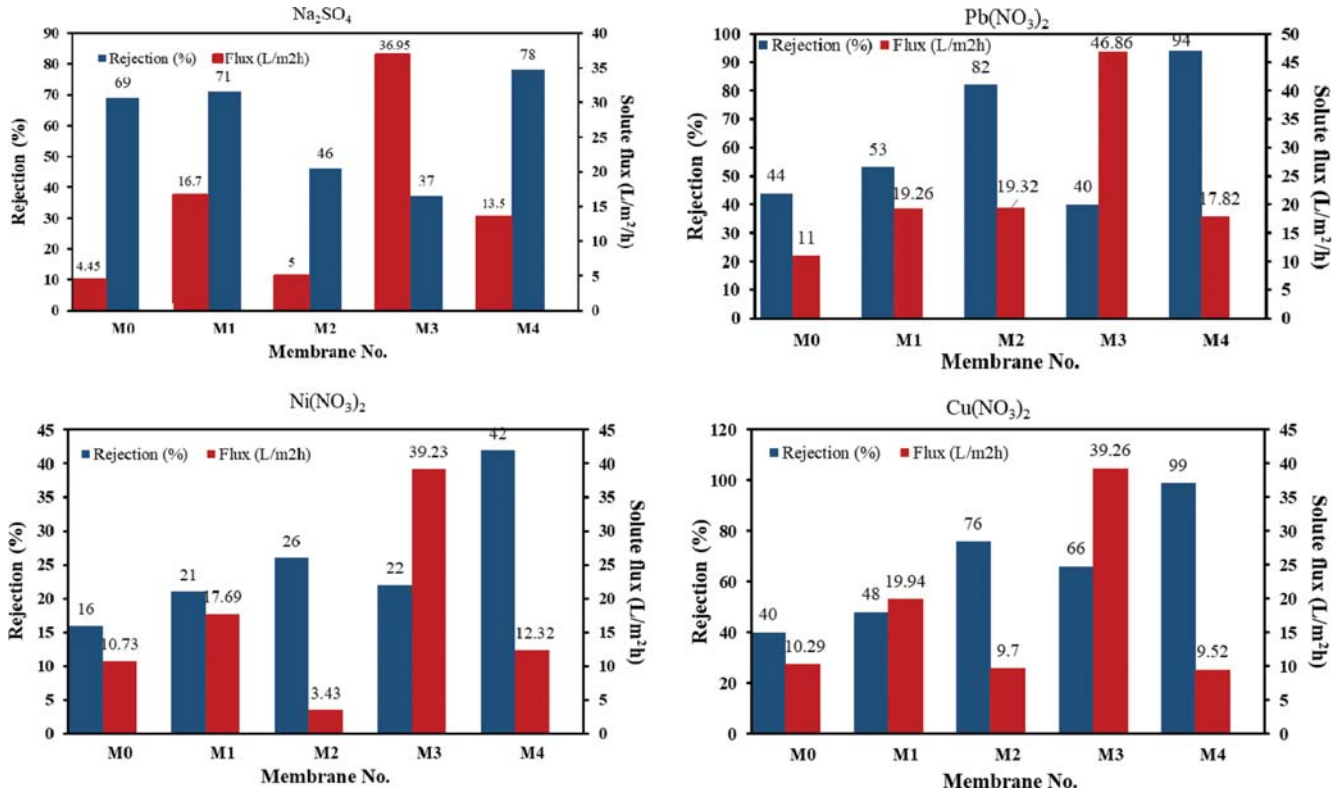

Fig. 10. Comparison between flux and salts rejection for the prepared membranes.

2-2. Salt Rejection of Prepared Membranes

The results of Na_2SO_4, $Pb(NO_3)_2$, $Ni(NO_3)_2$ and $Cu(NO_3)_2$ rejection for prepared membranes are shown in Fig. 8, Fig. 9 and Fig. 10, respectively. The results show highest rejection of Na_2SO_4, $Pb(NO_3)_2$, and $Cu(NO_3)_2$ salts solutions for the blended hybrid membrane containing 1 wt% of glycidyl-POSS, that were 78%, 94%, and 99%, respectively, whereas they measured 69%, 44%, and 40%, for pristine membrane. $Ni(NO_3)_2$ rejection improved from 16% for pure membranes to 96% in 0.1 wt% glycidyl-POSS. Because, the cubical and rigid shape of the POSS cages increases membrane ability for high retention of contaminants [42].

As shown, the Na_2SO_4 rejection was decreased initially from 69% in M0 to 37% in M3 due to increasing mean pore size and porosity, which led to passing of salt ions. Then, the Na_2SO_4 rejection was increased again to 78% in M4; that can be the result of sharply decreasing mean pore size at high concentration of glycidyl POSS. These results are in agreement with the values in Table 3 and Fig. 8. Dispersion of glycidyl-POSS in membrane matrix is another important factor that affects salt rejection. The suitable dispersion of glycidyl-POSS creates higher active sites for them. It should be considered that glycidyl groups in the membrane structure have negative charges which repulse the SO_4^{2-} ions. Thus, the electrostatic repulsion between negative charges into the membrane structure and SO_4^{2-} ions may be considered as major mechanism for Na_2SO_4 rejection.

The adsorption and desorption of materials by membranes depend on the type of membrane materials, the inherent properties of filtered materials, hydrophobicity, size, acid dissociation constant, potential to form hydrogen bonding and other interaction mechanisms [43,44].

However, Cu^{2+} solubility is high at high concentration, but the accumulation of Cu^{2+} is fast due to the presence of nitrate groups (NO^{3-}). Thus, the salt ions accumulation on the membrane surface increases the repulsion of similar-charge ions [47] and leads to Cu^{2+} rejection. The high rejection for Cu^{+2} also has been reported by different studies [48-50]. Moreover, the cage structure of POSS creates active sites for Cu^{2+} adsorption. Ni^{2+} and Pb^{2+} have a lower solubility at high concentrations. Thus, these ions sediment on the membrane surface at high concentration, which leads to concentration polarization and decreased separation performance [46].

Moreover, the reducing of rejection can be explained due to larger pore sizes of the membrane than solute molecules. But, increasing the rejection can be explained due to the saturation of adsorption sites of membranes by metal ions adsorption on the membrane surface [43,45,51,52]. By considering the covalent radius of $Pb^{2+}>Ni^{2+}>Cu^{2+}$, the rejection of Pb^{2+} increased from M0 to M2 and then decreased due to increased pore size of the membrane, especially in 0.1 wt%. However, the rejection of Pb^{2+} was enhanced again due to negative electrical surface charge and reduction of pore membrane size in 1 wt% as shown in Table 3. Thus, rejection of Pb^{2+} was increased due to accumulation Pb^{2+} and repulsion Pb^{2+} ions as shown in Fig. 9 [53-55]. Moreover, the Pb^{2+} adsorption by cage structure of POSS is another reason for the improvement of Pb^{2+} rejection.

The rejection of Ni^{2+} ions increased by increase of glycidyl-POSS in 0.01 wt% due to increase of the top layer thickness on the membrane surface (14.49 μm). Then it was reduced in M3 due to increase in membrane porosity. Also, the hydrated radius of Ni^{+2} should be considered for ion transport via the membrane. Then it increased at high concentration of glycidyl POSS due to increasing the adsorption sites by glycidyl POSS into the membrane.

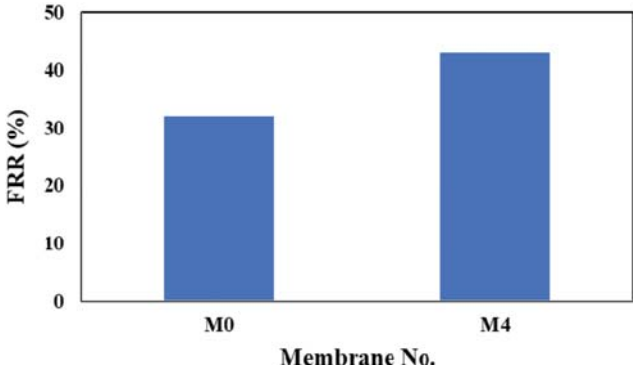

Fig. 11. Comparison of FRR% for different membranes; pristine membrane and the blended ones.

The Cu^{+2} rejection increased for M2 due to the increase of the membrane top layer thickness and increasing the adsorption sites with promoted the glycidyl groups. But the rejection of Cu^{+2} was decreased for M3; that can be as a result of increasing porosity and mean pore size and easy transport of Cu^{2+} ions. Finally, it increased to 99% due to tighter pores into the membranes.

Although, metal ions rejection is related to the mean effective diameter of membrane pores and hydrated diameters of ions [24,45], pH is another important factor that affects the metal solubility and metal ions rejection. In this study, pH was kept neutral. Therefore, salt ion rejection was not affected by the changes in pH.

The flux recovery ratio (FRR%) is illustrated in Fig. 11 after fouling and washing the prepared membranes for 120 min. According to Fig. 11, the highest FRR% was obtained for 1 wt% glycidyl POSS, which indicates the enhancement of antifouling properties in prepared membranes. Generally, improvement of antifouling properties can be explained by the enhancement of membrane hydrophilicity due to the affinity between membrane surface and water and reducing membrane roughness for M4 (1 wt% glycidyl POSS). These parameters are major reasons for the improvement of antifouling properties and higher FRR%. In fact, these reasons described decreasing contamination, adsorption or deposition foulants on the surface of the membrane, and foulants can be easily washed.

The results of this study compared to some commercial and earlier reported studies for removal of Na_2SO_4, $Pb(NO_3)_2$ and $Cu(NO_3)_2$ aqueous solutions as shown in Table 5. The separation performance of membranes related to different operation conditions and chemical properties of membranes. According to Table 5, the rejection of heavy metals by the fabricated membrane in this study is comparable to other studied membranes.

CONCLUSION

Blended PEI-based nanofiltration membranes were prepared by

Table 5. Comparison between the rejection for prepared membranes in this study and some commercial membranes and also earlier reported studies: Na_2SO_4, $Pb(NO_3)_2$ and $Cu(NO_3)_2$ aqueous solutions removal

Membrane	Nanoparticle	Nanoparticle loading (wt%)	Feed concentration (mg/l)	Pressure (bar)	PWF	Rejection (%)			Ref.
						Na^{2+}	Pb^{+2}	Cu^{+2}	
Torlon ®	GO[a]	-	-	3	-		81	-	[56]
Polyether sulfone	GO	0.5 wt%	1000	5	13.9 (kg/m^2·h)		-	84.8	[57]
Polyether sulfone	GO	1 wt%	1000	5	7.3 (kg/m^2·h)		-	77	[57]
HPEI modified GO&EDA framework membrane	GO framework	-	1000	1	5.01 (LMH bar^{-1})		95.7±0.7	-	[58]
Polyether sulfone	PANI/Fe_3O_4[b]	0.1 wt%	20	5	47 (kg/m^2·h)		-	85	[59]
Polyether sulfone	MWCNTs-PAMAM[c]	-	300	-	48 (L/m^{2}h)		89.9	97.1	[60]
PI84	GO	0.9 wt%	0.05 M	15	13.07 (L/m^{2}h)	100	-	-	[61]
Chitosan	NH_2-MIL-101(Al)	20%[d]	2000	-	-	20.53	-	-	[62]
Polyether sulfone	MMGO[e]	0.5 wt%	20	4	58 (kg/m^{2}h)	89	-	96	[63]
AFC 80	-	-	100	10	13 (L/m^{2}h)	-	98	-	[64]
NF 270 membrane in acidic medium	-	-	10	4.5	74.03 (L/m^{2}h)	-	87	-	[65]
PVC-ABA/PSf[f]		0.5 wt%	10	4.5	34.17 (L/m^{2}h)	-	68	-	[65]
PVDF	A-HNTs[g]	0.66 wt%	100	-	26 (L/m^{2}h)	-	-	47%	[66]
PEI/glycidyl POSS	-	1 wt%	1000	4.5	18 (L/m^{2}h)	78	94	99	In this study

[a]Graphene oxide (GO)
[b]Polyaniline/iron (II, III) oxide ($PANI/Fe_3O_4$) nanoparticles
[c]Multiwallet carbon nanotube-poly(amidoamine) (PAMAM) (MWCNTs-PAMAM)
[d]The weight loading of MOF was calculated by the following equation: $x=M_{MOF}/M_{Chitosan}*100\%$
[e]Metformin/GO/Fe_3O_4 hybrid (MMGO)
[f]Poly vinyl chloride (PVC)- 4-amino benzoic acid (ABA)/polysulfone (PSf)
[g]3-Aminopropyltriethoxysilane (APTES) grafted halloysite nanotubes (HNTs)

incorporation of glycidyl-POSS. The presence of epoxy groups in the glycidyl-POSS increased membrane hydrophilicity and negative charges on the surface of membrane. Donnan exclusion and/or adsorption mechanisms have an important role in the rejection of ion metals by nanofiltration membranes. The PWF and the antifouling property of blended membrane improved at 1 wt% glycidyl-POSS. The FESEM images showed a thicker top layer and with more porosity. The smoothest surface was obtained for M4. The separation performance of prepared membranes was evaluated for Na_2SO_4, Pb $(NO_3)_2$, Ni $(NO_3)_2$ and Cu $(NO_3)_2$. The rejection of salts improved due to more active sites. Among prepared membranes, M4 with 1 wt% glycidyl-POSS had the best performance. The antifouling properties enhanced for prepared membranes and the highest FRR% observed for the blended membrane containing of 1 wt% glycidyl-POSS.

ACKNOWLEDGEMENT

The authors gratefully acknowledge Arak University for the financial support during this research.

REFERENCES

1. E. Bagheripour, A. Moghadassi and S. M. Hosseini, *Korean J. Chem. Eng.*, **33**, 1462 (2016).
2. S. Ansari, E. Bagheripour, A. Moghadassi and S. M. Hosseini, *J. Polym. Eng.*, **37**, 61 (2017).
3. F. Amiri, A. Moghadassi, E. Bagheripour and F. Parvizian, *J. Membr. Sci. Res.*, **3**, 50 (2017).
4. X. You, H. Wu, Y. Su, J. Yuan, R. Zhang, Q. Yu, M. Wu, Z. Jiang and X. Cao, *J. Mater. Chem. A*, **6**, 13191 (2018).
5. S. Ansari, A. R. Moghadassi and S. M. Hosseini, *Desalination*, **357**, 189 (2015).
6. E. Bagheripour, A. Moghadassi and S. Hosseini, *Arabian J. Sci. Eng.*, **41**, 2545 (2016).
7. A. Azari, R. Rezaei and H. Sanaeepur, *Desalination Water Treatment*, **124**, 308 (2018).
8. H. Zhou, M. H. Chua and J. Xu, Functionalized POSS-based

hybrid composites, in: Polymer composites with functionalized nanoparticles, Elsevier, 179 (2019).
9. A. Kausar, *Polym. Plast. Technol. Eng.*, **56**, 1401 (2017).
10. E. Ayandele, B. Sarkar and P. Alexandridis, *Nanomaterials*, **2**, 445 (2012).
11. S. M. Hosseini, M. Afshari, A. R. Fazlali, S. Koudzari Farahani, S. Bandehali, B. Van der Bruggen and E. Bagheripour, *Chem. Eng. Res. Design*, **147**, 390 (2019).
12. X. Chen and L. F. Dumée, *Adv. Eng. Mater.*, **21**, 1800667 (2019).
13. N. Koutahzadeh, M. R. Esfahani, F. Bailey, A. Taylor and A. R. J. J. o. E. C. E. Esfahani, Enhanced performance of polyhedral oligomeric silsesquioxanes/polysulfone nanocomposite membrane with improved permeability and antifouling properties for water treatment (2018).
14. M. Dalwani, J. Zheng, M. Hempenius, M. J. Raaijmakers, C. M. Doherty, A. J. Hill, M. Wessling and N. E. Benes, *J. Mater. Chem. A*, **22**, 14835 (2012).
15. J. Duan, E. Litwiller and I. Pinnau, *J. Membr. Sci.*, **473**, 157 (2015).
16. S. C. Chen, X. Z. Fu and T.-S. Chung, *Desalination*, **335**, 17 (2014).
17. J. Sun, L. Wu and F. Hu, *RSC Adv.*, **5**, 40753 (2015).
18. X. You, T. Ma, Y. Su, H. Wu, M. Wu, H. Cai, G. Sun and Z. Jiang, *J. Membr. Sci.*, **540**, 454 (2017).
19. Y. Liu, C. Liu, X. Fu, O. Lin, Z. Wang, C. Wang and C. Zhang, *J. Membr. Sci.*, **586**, 211 (2019).
20. Z. Bahrami, A. Akbari and B. Eftekhari-Sis, *Int. J. Biol. Macromol.*, **129**, 187 (2019).
21. C. Lu, C. Su, H. Cao, X. Ma, F. Duan, J. Chang and Y. Li, *Mater. Lett.*, **228**, 85 (2018).
22. K. Yamamoto, S. Koge, T. Gunji, M. Kanezashi, T. Tsuru and J. Ohshita, *Desalination*, **404**, 322 (2017).
23. F. Zareei and S. M. Hosseini, *Sep. Purif. Technol.*, **226**, 48 (2019).
24. Y. He, Y. P. Tang and T. S. Chung, *Ind. Eng. Chem. Res.*, **55**, 12929 (2016).
25. A. C. Kucuk and O. A. Urucu, *React. Funct. Polym.*, **140**, 22 (2019).
26. R. S. Hebbar, A. M. Isloor, A. Ismail, S. J. Shilton, A. Obaid and H.-K. Fun, *New J. Chem.*, **39**, 6141 (2015).
27. R. S. Hebbar, A. M. Isloor and A. Ismail, *RSC Adv.*, **4**, 55773 (2014).
28. R. S. Hebbar, A. M. Isloor, K. Ananda and A. Ismail, *J. Mater. Chem. A*, **4**, 764 (2016).
29. A. Rahimpour, *Desalination*, **265**, 93 (2011).
30. Y. Mansourpanah, S. Madaeni, A. Rahimpour, A. Farhadian and A. Taheri, *J. Membr. Sci.*, **330**, 297 (2009).
31. E. Bagheripour, A. Moghadassi, S. Hosseini, B. van der Bruggen and F. Parvizian, *J. Ind. Eng. Chem.*, **62**, 311 (2018).
32. Y. W. Chang, E. Wang, G. Shin, J. E. Han and P. T. Mather, *Polym. Adv. Technol.*, **18**, 535 (2007).
33. J. Xia, S. Liu, P. K. Pallathadka, M. L. Chng and T.-S. Chung, *Ind. Eng. Chem. Res.*, **49**, 12014 (2010).
34. M. Moochani, A. Moghadassi, S. M. Hosseini, E. Bagheripour and F. Parvizian, *J. Chem. Eng.*, **33**, 2674 (2016).
35. E. Bagheripour, A. Moghadassi and S. M. Hosseini, *Int. J. Eng.*, **30**, 821 (2017).
36. N. Rakhshan and M. Pakizeh, *J. Ind. Eng. Chem.*, **34**, 51 (2016).
37. M. Safarpour, V. Vatanpour and A. Khataee, *Desalination*, **393**, 65 (2016).
38. H.-Z. Zhang, Z.-L. Xu, H. Ding and Y.-J. Tang, *Desalination*, **420**, 158 (2017).
39. S. Ansari, A. Moghadassi and S. Hosseini, *Desalination*, **357**, 189 (2015).
40. M. Sivakumar, D. R. Mohan and R. Rangarajan, *J. Membr. Sci.*, **268**, 208 (2006).
41. P. Mobarakabad, A. Moghadassi and S. Hosseini, *Desalination*, **365**, 227 (2015).
42. I. V. Gürsel, T. Noël, Q. Wang and V. Hessel, *Green Chem.*, **17**, 2012 (2015).
43. A. J. Semião and A. I. Schäfer, *J. Membr. Sci.*, **381**, 132 (2011).
44. W.-P. Zhu, S.-P. Sun, J. Gao, F.-J. Fu and T.-S. Chung, *J. Membr. Sci.*, **456**, 117 (2014).
45. N. Chitpong and S. M. Husson, *J. Membr. Sci.*, **523**, 418 (2017).
46. M. Maurer, W. Pronk and T. Larsen, *Water Res.*, **40**, 3151 (2006).
47. A. Z. Yaser, Development of integrated nanofiltration system for highly concentrated dye removal, in, Swansea University (2011).
48. B. Al-Rashdi, D. Johnson and N. Hilal, *Desalination*, **315**, 2 (2013).
49. J. Tanninen, M. Mänttäri and M. Nyström, *Desalination*, **189**, 92 (2006).
50. L. M. Ortega, R. m. Lebrun, J.-F. o. Blais and R. Hausler, *Desalination*, **227**, 204 (2008).
51. L. Nghiem and A. Schäfer, *Environ. Eng. Sci.*, **19**, 441 (2002).
52. M. Hua, S. Zhang, B. Pan, W. Zhang, L. Lv and Q. Zhang, *J. Hazard. Mater.*, **211**, 317 (2012).
53. B. Ganesh, A. M. Isloor and A. F. Ismail, *Desalination*, **313**, 199 (2013).
54. C. Bellona and J. E. Drewes, *J. Membr. Sci.*, **249**, 227 (2005).
55. V. Kochkodan and N. Hilal, *Desalination*, **356**, 187 (2015).
56. Y. Zhang, S. Zhang, J. Gao and T.-S. Chung, *J. Membr. Sci.*, **515**, 230 (2016).
57. N. Gholami and H. Mahdavi, *Adv. Polym. Tech.*, **37**, 3529 (2018).
58. Y. Zhang, S. Zhang and T.-S. Chung, *Environ. Sci. Technol.*, **49**, 10235 (2015).
59. P. Daraei, S. S. Madaeni, N. Ghaemi, E. Salehi, M. A. Khadivi, R. Moradian and B. Astinchap, *J. Membr. Sci.*, **415**, 250 (2012).
60. H.-Z. Zhang, Z.-L. Xu and J.-Y. Sun, *RSC Adv.*, **8**, 29455 (2018).
61. N. K. Zaman, R. Rohani, A. W. Mohammad and A. M. Isloor, *Chem. Eng. Sci.*, **177**, 218 (2018).
62. X.-H. Ma, Z. Yang, Z.-K. Yao, Z.-L. Xu and C. Y. Tang, *J. Membr. Sci.*, **525**, 269 (2017).
63. G. Abdi, A. Alizadeh, S. Zinadini and G. Moradi, *J. Membr. Sci.*, **552**, 326 (2018).
64. C.-V. Gherasim and P. Mikulášek, *Desalination*, **343**, 67 (2014).
65. V. Nayak, M. Jyothi, R. G. Balakrishna, M. Padaki and S. Deon, *J. Hazard. Mater.*, **331**, 289 (2017).
66. G. Zeng, Y. He, Y. Zhan, L. Zhang, Y. Pan, C. Zhang and Z. Yu, *J. Hazard. Mater.*, **317**, 60 (2016).